From Coherent Systems Technology to Advanced Fiber Sensing for Smart Network Monitoring

Christian Dorize, Sterenn Guerrier, Elie Awwad, *Member, IEEE,* Haïk Mardoyan, *Senior Member, IEEE,* and Jérémie Renaudier, *Senior Member, IEEE*

(Invited Paper)

***Abstract*—Coherent technology developed in the past decade for transmission over core optical networks has leveraged the fiber capacity with the introduction of polarization diversity I/Q modulation along with advanced signal processing. Meanwhile, Distributed Acoustic Sensing (DAS) over telecom infrastructure has recently gained interest, and its introduction in deployed optical networks for in-depth supervision becomes a desirable feature for telecom operators. This paper intends to show that the combination of coherent solutions and digital processing techniques implemented today in current transceiver systems can strongly benefit DAS technology: key performance parameters as sensitivity threshold and sensing range, and coexistence with data traffic can be significantly improved compared with the figures achieved by initially introduced conventional solutions.**

***Index Terms*—Acoustic sensors, digital signal processing, fiber optic sensors, optical fiber networks, smart cities, telecommunication network reliability.**

I. Introduction

DISTRIBUTED acoustic sensing (DAS) technology was recently introduced to detect and locate mechanical events along an optical fiber, thus transforming this medium into a sensor array mainly by exploiting the Rayleigh backscattering effect. The first fields of application were in the oil & gas industry typically for continuous monitoring of oil wells and gas pipelines to detect leaks or flow irregularities [1], for structural health monitoring to detect cracks, for the supervision of power cables to detect cable faults, and for monitoring sensitive perimeters [2]. In these fields, a dedicated fiber deployed along or within the structure conveniently replaces a large set of independent electrodynamic or piezoelectric sensors. In the meantime, optical fiber cables are the backbone of today's worldwide telecom network, with millions of kilometers of cables deployed over the globe, both terrestrial and submarine, to handle the internet traffic. These telecom cables cover a wide surface of terrestrial and subsea areas, which make them perfect candidates for acoustic sensing of the environment. Most of the research works targeting sensing through the telecom infrastructure have applied commercially available DAS solutions originally used over dedicated sensing cables. They had shown promising results in road/rail traffic supervision [3]–[5] and in measuring dynamics on the scale of an urban or regional area: near-surface characterization [6], [7] detecting high levels of anthropogenic activities of certain sites during crisis (as in the recent COVID19 period) [8], [9], and other seismic events.

Beyond these promising results, we believe that the integration of sensing capability within the data communication infrastructure can be drastically improved with coherent technology. The objective of this paper is twofold: firstly, we show how to customize transceiver technologies used today in optical fiber transmission systems to build an advanced digital DAS system. We emphasize particularly on the benefits offered by polarization diversity and frequency diversity such as the achievement of very low noise floors. We also bring up digital probing code structures based on Golay sequences, constant amplitude zero autocorrelation (CAZAC) codes or linear frequency sweeps. Secondly, we demonstrate that the proposed probing technique based on continuous codes can coexist with data traffic operated on adjacent Wavelength Division Multiplex (WDM) channels without any impact on the quality of data transmission. Therefore, a wide range of novel DAS applications exploiting the already deployed telecom infrastructure can be envisaged, from in-depth monitoring of telecom operator networks for more automation and enhanced telemetry [10] to new markets driven by smart city applications. Before concluding, we briefly review recent works on acoustic sensing over the optical fiber infrastructure based on information extraction from the forward propagating light signal, and we point out that both DAS and forward sensing based solutions offer complementary advantages to smart network monitoring.

II. Channel estimation with polarization diversity codes

Pulsed light from a single-wavelength laser is the most straightforward probe signal in terms of optical generation, and each transmitted pulse yields straight access to one backscattered response of the fiber sensor over distance. Similarly to light which is transmitted from one fiber end to the other, the probing pulses experience attenuation along distance, and so does the backscattered light. The sensing system is therefore limited by the detector sensitivity on the one hand, and by the maximum launchable power on the other hand, as signal distortions and non-linear interference may arise when sending

C. Dorize (corresponding author), S. Guerrier, H. Mardoyan and J. Renaudier are with Nokia Bell Labs, route de Villejust, 91620 Nozay, France. (e-mails: christian.dorize@nokia-bell-labs.com, sterenn.guerrier@nokia-bell-labs.com, haik.mardoyan@nokia-bell-labs.com, jeremie.renaudier@nokia-bell-labs.com)

E. Awwad is with the Department of Communications and Electronics of TELECOM Paris, 16 place Marguerite Perey, 91120 Palaiseau (e-mail: elie.awwad@telecom-paris.fr)

Manuscript received May 31, 2022; revised XXX MM, YYYY.

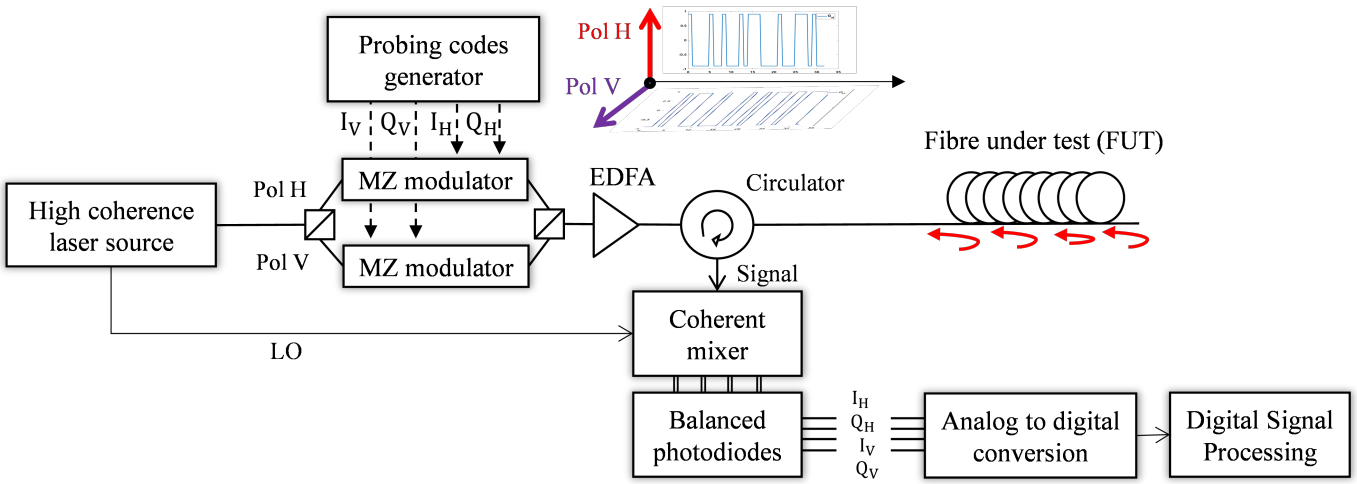

Fig. 1. DAS experimental set-up with polarization diversity both at transmitter and receiver sides (Coherent-MIMO). MZ: Mach-Zehnder, LO: Local Oscillator, EDFA: Erbium Doped Fiber Amplifier.

high optical power through the fiber sensor, such as non-linear Kerr and scattering effects in the fiber [11]. To avoid high peak power levels, the interrogation pulse can be widened : spread-pulse or spread-spectrum techniques are alternatives to launch higher power probing signals in the fiber and so to relax the conditions on the maximum peak power and detector sensitivity. The authors developed a purely digital polarization-multiplexed spread-pulse probing technique, summarized in the section below.

A. Dual polarization probing with continuous codes

Probing stage may rely on specific binary sequences [12] or random data coded over a constant-modulus constellation thanks to optical communication modulators such as Quadrature Phase Shift Keying (QPSK) [13]. These sequences exhibit Dirac-like autocorrelation that allow to recover the system impulse response after digital signal processing at the receiver side. For DAS applications, these alternatives to probing pulses are usually transmitted onto a single polarization axis. In [14], we introduced instead a probing technique based on mutually orthogonal binary codes derived from Golay sequences that simultaneously modulate, by means of a Dual Polarization (DP) Mach Zehnder modulator, two orthogonal polarization states of a continuous light signal. At the receiver side, a DP coherent receiver, as the one usually used in long haul optical fiber communication systems, captures the back-scattered optical field. In an SMF, the backscattered signal vector $\mathbf{E_r} = \begin{pmatrix} \mathbf{E}_{rx} \\ \mathbf{E}_{ry} \end{pmatrix}$ is given by $\mathbf{E_r} = \mathbf{H_{i,j}E_t}$ where $\mathbf{E_t} = \begin{pmatrix} \mathbf{E}_{tx} \\ \mathbf{E}_{ty} \end{pmatrix}$ is the transmitted symbol-vector onto each of two orthogonal polarization axes x and y, $\mathbf{H}_{i,j}$ is the dual-pass backscattered channel response up to the i^{th} fiber segment at time index j represented by a 2×2 Jones matrix. At the receiver side, the analog-to-digital converters (ADCs) used in our experiments are commercially available digitizers with 16-bit vertical resolution, 500 MSamples/s sampling rate and a 350 MHz analog bandwidth. The applied digital signal processing (DSP) consists in normalization and re-sampling of the four signals acquired from four ADCs (in-phase and quadrature beat terms of each of the two orthogonal polarization states), correlation with the transmitted sequences, and synchronization. Block processing of the acquired data may be used to perform the correlations for real-time implementations. Synchronization can be implemented by detecting a reference reflection in the back-scattered channel response followed by a framing of consecutive responses. A set of matrices $\mathbf{H}_i$ is derived periodically at time index j by means of four correlations between each of the two received optical fields $\{\mathbf{E}_{rx}, \mathbf{E}_{ry}\}$ and each of the two transmitted codes $\{\mathbf{E}_{tx}, \mathbf{E}_{ty}\}$.

The design of the mutually orthogonal probing codes $\mathbf{E}_{tx}$ and $\mathbf{E}_{ty}$ is based on a recursion from a 4-symbol seed of alphabet $\{+1, -1\}$ to get the desirable length, yielding a probing code duration $T_{code} = 2.(4.2^K)/F_{symb}$, where K is the recursion index and F_{symb} is the symbol rate. When continuously probing the fiber with the period T_{code}, the line is analyzed within a mechanical bandwidth $BW = 1/(2.T_{code})$ (The mechanical bandwidth or the DAS response bandwidth, is defined as the highest frequency that can be detected in the measurand or the Nyquist frequency, i.e. half the probing rate [15]), whereas the spatial resolution $S_r = c_f/(2.F_{symb})$ is adjusted through the symbol rate, c_f standing for the light velocity in the fiber core.

The specific orthogonality properties between the designed codes guarantee the mathematically perfect channel estimation provided that a suitable sequence length is chosen: T_{code} must verify $4.T_{rtd} < T_{code} < T_{coh}$ where $T_{rtd} = 2.L/c_f$ stands for the round-trip delay in a fiber of length L and T_{coh} is the coherence time of the laser source. To ensure that the channel remains stationary, $T_{code} < T_{coh}$ guarantees that the reference phase is almost constant over the duration of a single code, and the condition $4.T_{rtd} < T_{code}$ is necessary to avoid the overlapping of successive fiber estimations (channel impulse responses) after correlation at the reception. This specific DP $\Delta\phi$-OTDR system is referred to as Coherent-MIMO [16] to highlight the polarization diversity used both at the transmitter

and at the receiver sides. An outline schematic of the Coherent-MIMO-OTDR is displayed in Figure 1.

Therefore, probing an optical fiber on two orthogonal polarization axes with the designed binary codes formally yields unbiased estimations of the full Jones matrices $\mathbf{H}_{i,j}$ of segments of the sensed fiber with a spatial resolution S_r and refresh rate T_{code}. Indeed, the Jones representation describes an optical system as a succession of retardation plates and partial polarizers that operate on the incoming light [17]. The backscattered intensity, phase, and state of polarization (SOP) are so retrieved, and related information can be illustrated as we show in Figure 2. The absolute optical phase is extracted

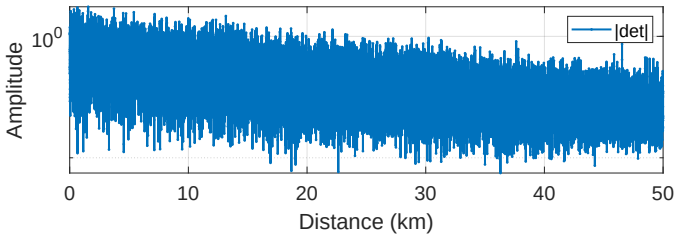

(a) Rayleigh backscattered intensity from a 50 km SMF spool, in static conditions

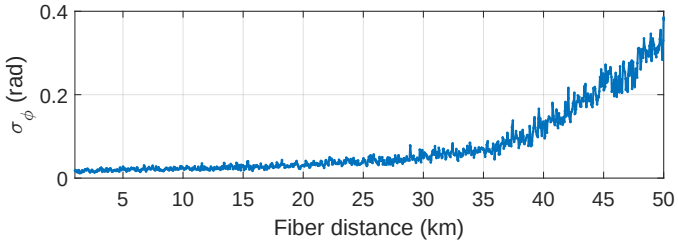

(b) standard deviation of differential phase along distance from a 50 km SMF spool, in static conditions

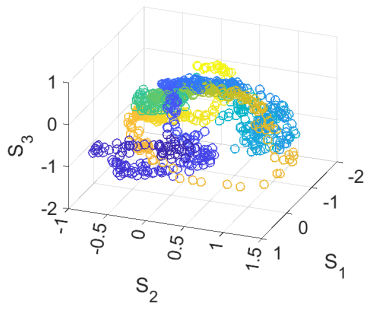

(c) Evolution of backscattered SOP over the Poincaré sphere, 347 m from the start of a 1km-long deployed fiber, during a disturbance caused by displacement of a manhole cover above a deployed fiber

Fig. 2. Example outputs from a backscattered Jones matrix.

from each matrix $\mathbf{H}_{i,j}$ as $\phi_{i,j} = 0.5\angle(\det \mathbf{H}_{i,j})$ where $\det(.)$ stands for the determinant operator. Having computed the absolute phases up to the i^{th} segment, the phase evolution per segment is obtained from the differential phases with the phase from the first reflector (usually a calibrated reflection at the interrogator's output) set as a reference. Figure 2(a) and (b) show the backscattered intensity from a 50 km SMF spool interrogated under static conditions in the lab, by means of a highly coherent laser source and the corresponding standard deviation of phase, respectively. Although the backscattered state of polarization (SOP) doesn't change much under static conditions, Figure 2(c) shows a backscattered SOP evolution from a field measurement [18].

B. Mitigation of polarization fading

To thoroughly understand the distributed acoustic sensors, exploration of both the fiber sensor and the active interrogator is needed. We modelled a distributed acoustic sensor considering a two-dimensional dual-polarization fiber model for transmission and backscattering of light in the fiber that allowed to anticipate DAS performances relative to fiber length and laser phase noise [19]. The Jones matrix response corresponding to the round trip up to segment index i is modeled as $\mathbf{H}_i = A_i p_i \mathbf{V}_i$, where $\mathbf{V}_i$ is a unitary matrix enclosing forward and backward evolution of the SOP of light, and A_i and p_i are, respectively, the attenuation and phase of the Rayleigh-distributed backscattered field at segment index i. In addition, a study on polarization diversity performance was conducted [16]: while most studies on polarization diversity in DAS focused on the (coherent) receiver [13], [20], the recent study demonstrated how input-polarization-induced phase noise also impacts the stability of backscattered phase estimations. In Figure 3, we show a comparison of phase stability simulations on 50 km single mode fiber for three interrogation schemes: Single Input polarization and Single Output (SISO), Single Input Multiple Output (SIMO) and Multiple Input Multiple Output (MIMO), "multiple" referring to dual-polarization here.

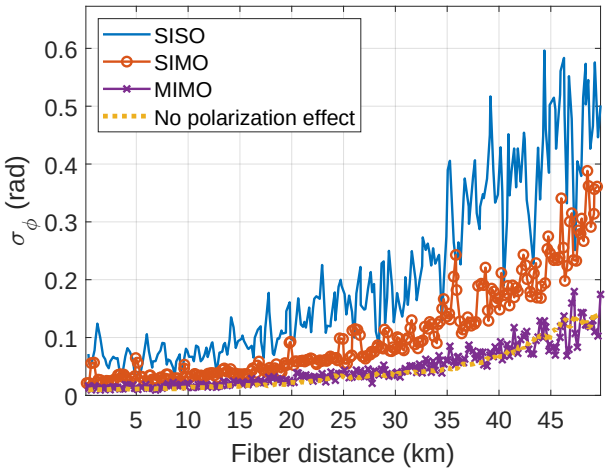

Fig. 3. Phase standard deviation σ_ϕ along distance, laser linewidth $\Delta\nu = 75$ Hz, 50 km fibre simulations. Averaged simulations along 50 km with coarse 200 m spatial sampling resolution [16].

The used noise-floor criterion is the standard deviation of the differential phase along the fiber in static conditions, which defines the detection threshold of the system. The first observation is the clear decrease of this threshold as the polarization diversity is introduced to the interrogator. The simulated performance for "no polarization effect" is included as well in Figure 3: this latter simulation was done with no polarization rotations or retardation in the fiber sensor and yields a phase standard deviation with the same profile as for

MIMO interrogation, hence highlighting that MIMO interrogation in a $\Delta\phi$-OTDR sensor is polarization-independent. These simulation results were also validated experimentally in [16].

III. A RELIABILITY CRITERION TO LOCATE COHERENT NOISE

Beyond polarization fading, coherent fading (also known as Rayleigh fading or speckle noise) [21] is another major issue which affects the performance of DAS systems. This effect originates when randomly spread elementary scatterers lead to destructive interferences of coherent light. Indeed, a highly coherent wave is required for the phase retrieval in our scheme, yet this same highly coherent wave is prone to encounter coherent fading as it passes through the random scattering zones of a fiber. At local intensity drop positions i, noise contribution becomes dominant in the estimated channel response $\mathbf{H}_i$, which severely degrades the phase estimation. Thus, it is of major importance to detect these local intensity drops to distinguish them from the true phase response of the sensor.

In MIMO mode, the backscattered intensity $|A_i.p_i|^2$ can be derived from the 2×2 matrix $\mathbf{H}_i$ by two estimators:

$$\hat{I_1} = |A_i.p_i|^2 = 1/2.|\mathbf{H}_i|^2_{frob} \text{and} \hat{I_2} = |A_i.p_i|^2 = |det(\mathbf{H}_i)|$$

The former one is the Frobenius norm of $\mathbf{H}_i$ while the latter one is the modulus of its determinant. They both perfectly estimate the intensity of the backscattered optical field. However, in presence of additive noise, they show distinct behavior [22] the $|\det|$ criterion provides a significantly smaller bias compared with the Frobenius one when the SNR decreases, as highlighted in Figure 4(a). We superimpose the SIMO intensity estimator, where the intensity is estimated by summing up the square modulus of the complex term of one column of the Jones matrices. It shows a 2 dB additional bias compared with the MIMO case at high SNR, but intensity biases provided by SIMO and MIMO Frobenius cases converge when the noise term becomes dominant. In summary, $|det(\mathbf{H})|$ is the most reliable estimator of the backscattered intensity and is preferable to account for local drops induced by coherent fading. Figure 4(b) displays the differential phase as a function of time measured experimentally at one fiber segment that is mechanically perturbated by a 15 Hz sine wave generated by a fan placed approximately 5 meters away from a 1.2 km fiber cable. Note that low-frequency vibrations can propagate on long distances and also through relatively thick surfaces (ground...), so no acoustic fading is expected here. The related intensity derived from the $|\det|$ criterion is superimposed, and we observe that it is modulated by the captured excitation which slightly modifies the initial position of the elementary scatterers and so modulates the intensity term $|A_i.p_i|^2$. The sine wave excitation is quite well captured by the phase response though local artifacts are present. Notice that the artifact locations observed in the phase response coincide with the local minima of the $|\det|$ metric. This correlation is not perfect as this intensity estimator is slightly biased at low intensity levels, and so false positives or negatives cannot be excluded. Nevertheless, it highlights that such artifacts are

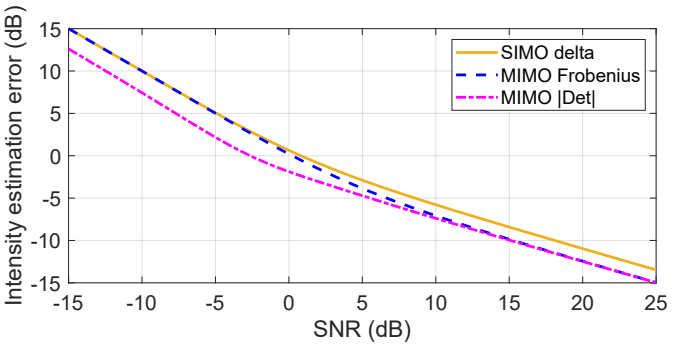

(a) Error estimation on intensity as function of SNR

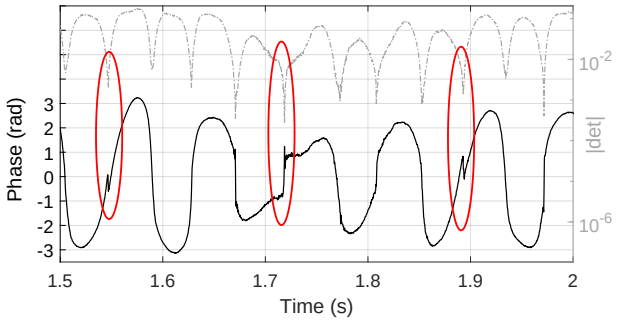

(b) Differential phase backscattered from a 2-meter perturbated fibre segment and superimposed $|\det|$ values. Red circles show artifacts in phase and the related backscattered intensity

Fig. 4. Intensity error estimation and relation with phase artifacts.

erroneous phase estimates that occur when the Jones matrix intensity drops. Therefore, the $|\det|$ metric can be exploited in MIMO sensing, on top of a fair intensity estimator, as a reliability index of the underlying estimated phase value, so behaving as a soft decision metric [22].

Beyond its detection and localization, the Rayleigh fading effect can be mitigated thanks to frequency diversity schemes [23], [24] at the cost of increased setup complexity. To avoid increasing measurements or processing time, several groups proposed low-cost approaches either to discriminate the false alarm peaks induced by the fading effect [25] or select a lower resolution set of backscattered points, chosen on a signal-to-noise ratio basis [19]. The next section proposes instead a low complexity and purely digital frequency diversity approach to mitigate coherent fading based on a multicarrier technique that is widely used in wireless communications.

IV. SPECTRAL DIVERSITY THROUGH OFDM CODING FOR COHERENT NOISE MITIGATION

Now that polarization diversity has resolved polarization-related fading effects, we are interested in benefiting from an additional degree of freedom to mitigate coherent fading in DAS. Coherent fading induces a degradation of the DAS performance at random 'blind' almost-zero-reflecting locations in the sensed fiber. Diversity-based solutions are an interesting scheme to overcome coherent fading. Spatial diversity and frequency diversity are the most popular schemes in DAS. Knowing that the random fading locations depend on the summation of phasors with random intensity and phase values, they rely on a combination of channel impulse response

estimates coming from separate probing signals at different frequencies, or from several consecutive fiber segments [26]. Some elegant works have recently demonstrated the mitigation of coherent fading by tracking the most reliable probe frequency in time [28], by combining probe signals simultaneously sent over different subcarriers [29], or by sending several frequency-shifted pulses [24]. Most investigated frequency-diversity based schemes require associated optical setups that are relatively complex or hard to fine-tune. In [27], we proposed to exploit a Rayleigh phase pattern diversity through an all-digital DP orthogonal frequency division multiplexing (OFDM) scheme. Identical DP probing codes are multiplexed in parallel over OFDM subcarriers and are sent simultaneously in the fiber. Hence, at the receiver side, this MIMO-OFDM interrogation scheme yields one Jones matrix response per code, per subcarrier and per segment. The coherent fading is mitigated by combining the estimations from the different subcarriers such that the $|\det|$ metric of the combined matrix is maximized. The results in [27] show that the OFDM interrogation along with the subcarrier combination performs an averaging on the system noise and thus significantly enhances the overall event-distinction threshold as we can clearly see in Figure 5. In this study, a single-carrier and an OFDM interrogation were compared for the same occupied electrical bandwidth, which means that the spatial resolution of each scheme was necessarily different. In that respect, the choice of the number of subcarriers should result in a trade-off between the noise floor reduction and the required spatial resolution.

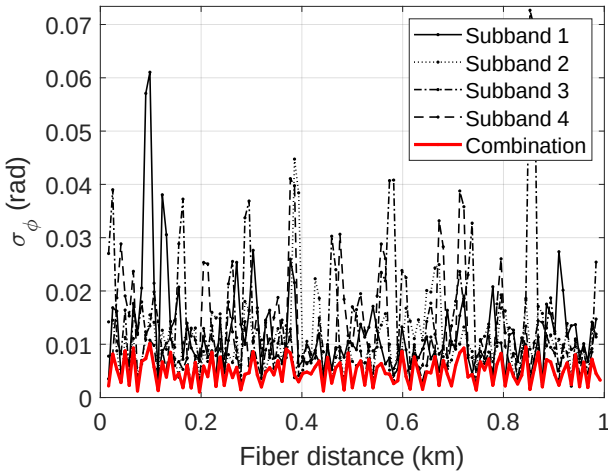

Fig. 5. Illustration of noise-floor reduction thanks to the combination of phase estimates from four OFDM subcarriers (static conditions) [27].

Hence, we showed that a digital multiplexing technique can be used to harness diversity and mitigate coherent fading. We believe that OFDM is a powerful tool for highly sensitive DAS systems and further benefits can still be obtained from it.

V. Probing codes alternatives

Field test conditions and product integrations have inherent limitations, whether induced by the shorter coherence lengths of laser sources used in telecom transceivers, or mechanical noise in the surroundings, or insertion losses connecting the $\Delta\phi$-OTDR system to the transponders or amplifier cards. Given these limitations, Golay-based codes for coherent-MIMO interrogation are not always the best option for practical use-cases. In the following, we present other probing options, namely coded frequency sweeps, over single or dual polarization. Although there are other DAS implementations that extract the differential phase by transmitting pulses and detecting the backscattering with a single photodiode, we do not cover them in detail as alternatives for Golay-based codes mainly because of their pulsed nature. For instance, two pulse-based DAS implementations that can retrieve phase information were suggested in the literature: chirped pulses through the current control of the laser [30] or phase-modulated dual-pulses [31]. Both operate with a direct detection at the receiver side. However, pulsed interrogation requires high energy pulses to achieve a good sensitivity over long distances, which makes it unsuitable for a co-existence of sensing with data transmission over a single fibre (unless important guard bands are introduced to avoid non-linear crosstalk as shown in [32]).

A. Release the constraint on the code length to enlarge the mechanical bandwidth of the sensor

Frequency sweep interrogation has been used for decades to measure the impulse response of systems to circumvent limitations of pulse interrogations. For fiber sensing applications, a digitally generated chirp signal that modulates the laser source after analog conversion is a flexible alternative to an AOM, which simplifies the optical setup of the interrogator. Also, CAZAC (Constant Amplitude Zero Autocorrelation) sequences, commonly used to estimate communication channels, approximate a linear frequency sweep signal by means of a complex-valued sequence with constant amplitude [33]. They can be implemented as well in a DAS system: the frequency modulation used for the former digital sweep is replaced by a PSK modulation.

Based on these two classes of digital chirps, we proposed in [34] interrogation alternatives to binary codes. A first sweep signal is used to cover linearly and uniformly the $[0 : F_{symb}/2]$ bandwidth over a period T_{sweep} for the first polarization and a second identical signal, but circularly shifted by half the sweep period, modulates simultaneously the orthogonal polarization. As for binary codes, the DP probing sweeps are repeated continuously, and they also yield formally perfect channel estimation under a Jones matrix form. However, perfect estimation is achieved with chirp signal lengths at least twice the roundtrip time in the sensed fiber instead of four times with the binary codes : the requirement for digital sweep interrogation is therefore $2.T_{rtd} < T_{sweep}$ while we had $4.T_{rtd} < T_{code}$ in section II.With amplitude modulated sweeps, imperfect transition between successive sweeps degrades performance in practice. When using CAZAC generated sweeps instead, the constant amplitude of symbols in the CAZAC sequence avoids any abrupt amplitude or frequency change issue. The symbol alphabet size is $M = log_4 N$ where N is the length of the CAZAC sequence. However, with sequence lengths compatible with sensed fiber links longer than one km, the modulation size M gets higher, and the generation of the phase modulation becomes more sensitive to the imperfections of the optical modulator.

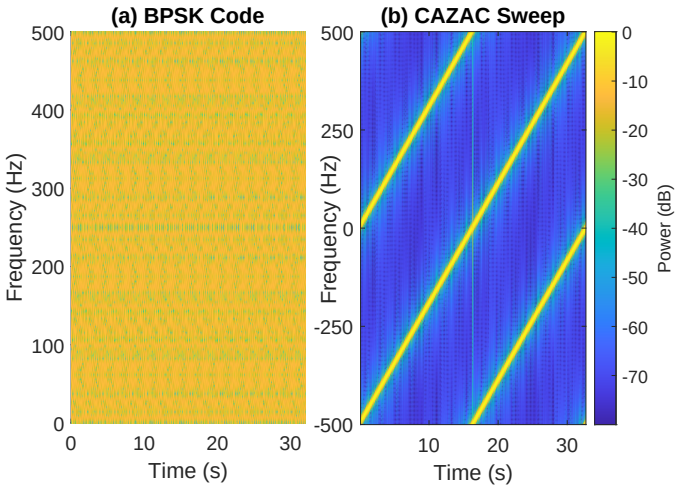

Fig. 6. Energy distribution in the time-frequency planes of DP-BPSK(a) versus DP-CAZAC(b) codes [34].

Figure 6 compares the initially introduced DP binary codes with the CAZAC codes by showing their respective energy distribution in the time versus frequency plane over one code period. For each case, the signatures at each of the two polarization axes are superimposed. The two circularly shifted linear sweeps of the CAZAC case are clearly reflected in Figure 6(b). Conversely, Figure 6(a) shows that binary probing codes probe the channel in a different way, with a signature homogeneously spread in the time-frequency plane.

B. Laser coherence length

Obviously, the longitudinal profile of the Rayleigh backscattered intensity is dependent on the probing laser linewidth. Besides, the statistic of backscattered intensity depends on the probing pulse length [35], where shorter pulses ensure the acquisition of higher contrast regardless their degree of coherence. Meanwhile, spread-pulse techniques require stationarity of the channel response, along with coherence state, during the full duration of a code [14]. Therefore, any degradation of the laser coherence leads to specific noise which we refer to as "laser phase noise" since it implies source phase fluctuations.

We reported in [19] how an increase of the laser linewidth from several Hz could degrade the detection threshold of the $\Delta\phi$-OTDR system especially after several kilometers distance, so decreasing the overall reach of the system. Consequently, working with constrained laser coherence requires to adapt the probing signal duration to account for the degradation of the $\Delta\phi$-OTDR interrogation. Since shortening the duration of a probing code necessarily decreases the reach of the sensor, alternative coded sequences as described above are to be employed when dealing with laser coherence limitations.

We pointed out, in the previous section, that polarization-independent MIMO probing signals, binary codes and digital sweeps, impose longer minimal probing time than the physical limit T_{rtd}, by factors of 4 and 2 respectively, which is somehow the price to pay to get rid of the polarization fading effect. Furthermore, switching to a single-polarization sweep allows to reach the minimal probing time of T_{rtd}. Notice that increasing the probing time has a positive impact on the system noise floor whereas decreasing it allows for a sensing analysis over an enhanced mechanical bandwidth. Figure 7 displays a comparison of the different impulse response spread depending on the method used to probe a same fiber length: it shows the aliasing patterns induced by each of the two MIMO probing techniques, thus highlighting their respective constraint regarding the minimal time length to achieve a perfect estimation of the backscattered channel. Therefore,

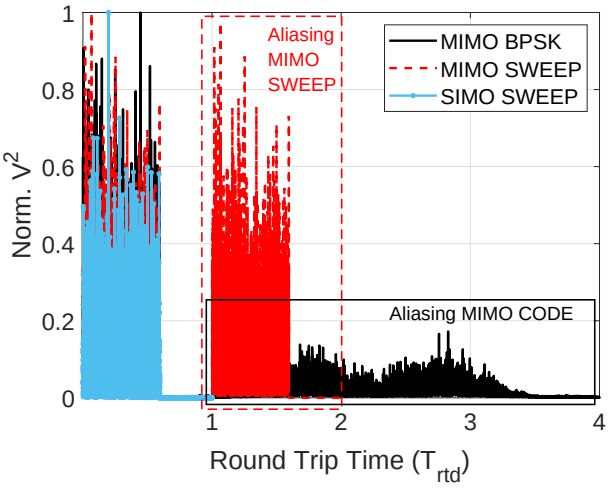

Fig. 7. Interrogation of a 10-km SMF with binary codes and linear frequency sweeps, MIMO and SIMO for the latter. The true fiber response spreads between 0 and 1.T_{rtd}.

when using a laser source featuring a given coherence time, the probing signal choice may be viewed as a degree of freedom to adapt to the length of the optical line to sense. Though MIMO sensing offers the best performance in terms of detection threshold, turning back to SIMO interrogation with a digital sweep remains a fair solution when the line length approaches the coherence length of the source.

C. Coexistence between sensing and data transmission

One last, yet fundamental aspect of DAS in telecommunication is its operability jointly with live data transmission. For best noise-floor performance, probing pulses in DAS systems exhibit high peak powers and would interfere with data channels due to fiber nonlinearity if they were co-propagating. This explains why it is sometimes claimed in the literature that $\Delta\phi$-OTDR can only be performed on dark fibers in telecom networks. As network resources could become scarce with the constant traffic increase, the coexistence between sensing and data transmission is now under interest. For example, counter propagating DWDM (Dense Wavelength Division Multiplexing) signals and probing pulses has recently been investigated [36]. Coming back to spread-pulse techniques, probing codes continuously probe the sensing channel, which in turns reduces the Peak-to-Average Power Ratio (PAPR), thus mitigating non-linear induced distortions on surrounding DWDM channels. It is possible to load the sensing channel with an average channel power comparable to the adjacent transmission slots, namely close to 0 dBm, and yet obtain satisfactory backscattered intensity level after correlation.

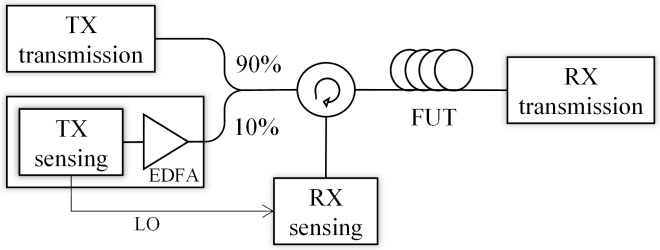

(a) Outline schematic of data-sensing coexistence set-up

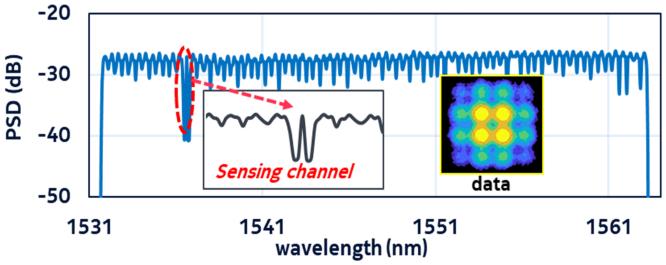

(b) Transmitted C-band data alongside with sensing channel in ITU 51 band

Fig. 8. Co-propagation of sensing channel and DWDM data in telecommunication C-band: set-up and transmitted optical Power Spectral Density (PSD).

(a) Location of the measure and position of the deployed fiber cable in tunnel (highlighted cable)

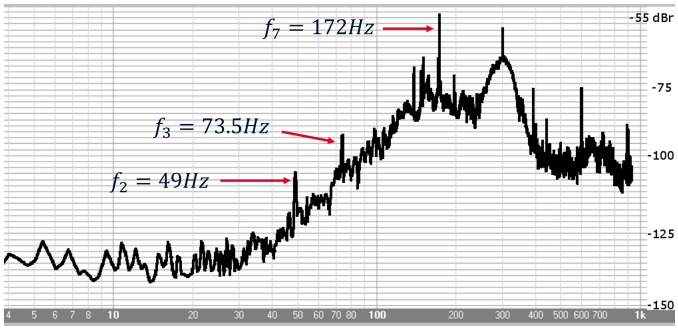

(b) Power spectral density (PSD) of differential phase at 81km from the fiber start (microphone measurement)

Fig. 9. Cable under test and measured acoustic perturbation.

In [37], the non-intrusive coexistence between transmission of DWDM channels carrying 600 Gb/s DP-16QAM data and a coded sweep sensing signal was demonstrated. The outline schematic of the experiment and the transmitted spectrum are displayed in Figure 8(a): the sensing signal is coupled to the transmitted C-band channels through a 10/90 optical coupler, the sensing probe power is adjusted such that the power of the sensing signal in ITU-C51 slot is similar to that in other WDM slots used for transmission. At the sensing receiver, the backscattered light is captured at the launching end of the fiber span where self-homodyne configuration of the coherent receiver measures the signal backscattered from the sole sensing slot. In Figure 8(b), we show the full C-band transmitted data, except for ITU-C51 DWDM slot enclosing the sensing signal. The WDM channels adjacent to the sensing one are two channels under test (CUTs). The CUTs carry 90 GBd DP-16QAM and the 82 loading channels with a 50GHz spacing are modulated at 49 GBd with DP-16QAM, for an overall link capacity of 27.85 Tbit/s over a single fibre. The detail of the DWDM testbed composition is given in [37].

The digital sensing interrogator probes the full span at a rate F_{symb} using single polarization digitally generated linear frequency sweep signals, covering a $[0 : F_{symb}/2]$ bandwidth over a period $T_{sweep} \geq T_{rtd}$. As described in section V, coded sweep is formally less efficient than coded bipolar sequences ; yet it allows to reduce the constraint on the coherence length of our laser source to cope with the long sensing distance demonstrated in this experiment, as the SIMO probing requires a laser source coherence restricted to the sole fiber round-trip time T_{rtd}.

Another positive effect of the relaxed condition on the probing signal duration is the increase of the mechanical bandwidth $BW = 1/(2.T_{sweep})$ (where $T_{sweep} = 0.25T_{code}$ for the same sensing fiber length). In the experiment, the 82-km fiber under test is interrogated at $F_{symb} = 50$MBaud, with T_{sweep}= 0.8 ms, yielding a 600 Hz mechanical bandwidth. The fiber under test (FUT) consists of 80 km Single Mode Fiber (SMF) spools (one 30 km spool and one 50 km spool) and a 1.4 km long cable deployed between two buildings, fixed to the wall of a tunnel, and located 0.6 m under an asphalt road. Figure 9(a) shows a picture of the cable position in the tunnel. The main perturbation on the line is an air conditioning system 10 m distant from the deployed cable and located near the second building. Acoustic measurements (sonometer and spectrum analyzer) showed a stable low acoustic pressure of 63 dB_C SPL at the cable with a spectral signature made of a 24.5 Hz fundamental component and harmonics up to the seventh rank (172 Hz), as displayed in Figure 9(b).

Three different configurations were investigated: the fiber spools were either connected before the deployed fiber section, or 30 km SMF were placed before the deployed fiber section and 50 km after, or else the full 80 km were connected after the deployed cable. Thus, the acoustic disturbance was measured at three different fiber distances. Detection and localization of the acoustic disturbance after 80 km is displayed in Figure 10(a): a peak of phase variations is visible above the detection threshold of cumulated phase noise of the backscattered light after 80 km. Figure 10(b) is the power spectral density of the differential phase at the detection peak (in each of the three configurations mentioned earlier). It gives the spectral signature of the air conditioning machinery, and it is in line with the previously measured spectral signature (in Figure 9(b)). After 81 km, the fundamental and third order harmonic are visible on the spectrum, exceeding the noise level by nearly 10 dB.

Finally, we analyze the performance of the adjacent coherent

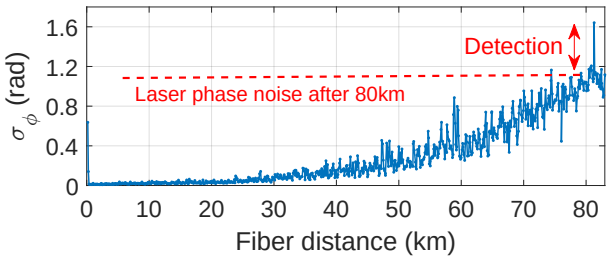

(a) Optical phase standard deviation σ_ϕ along distance: detection and localization

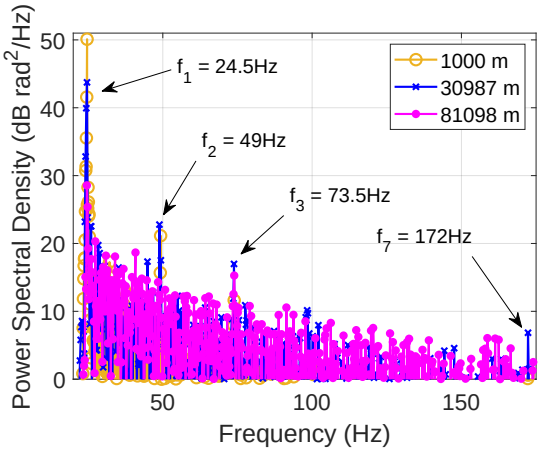

(b) PSD of differential phase at 81km from the fiber start

Fig. 10. Detection, localization, and identification of an acoustic perturbation on an 82-km long SSMF.

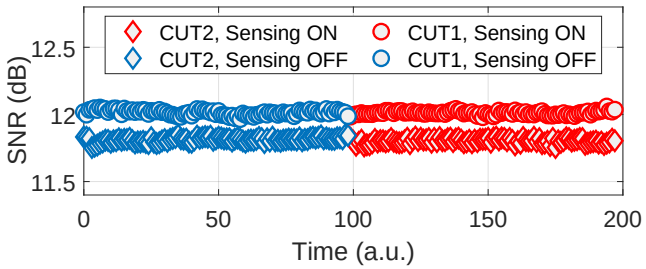

(a) Measured pre-FEC SNR of CUTs with and without adjacent sensing signal

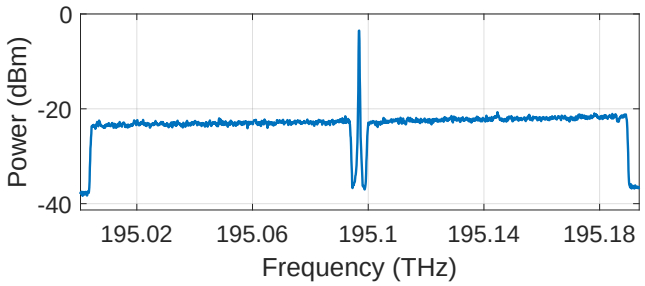

(b) Optical spectrum of CUTs spaced 2GHz apart from the sensing signal

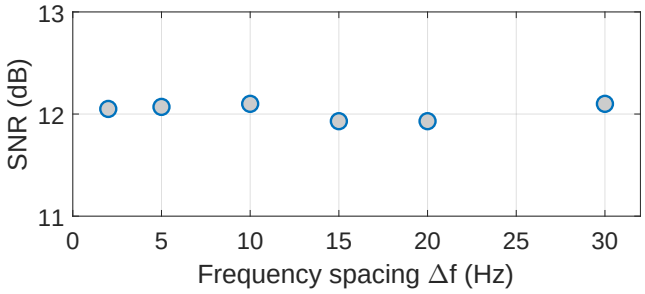

(c) Measured performance of CUT2 vs. frequency spacing

Fig. 11. Data transmission performance in presence of a sensing signal: pre-FEC SNR measurements.

channels carrying 600 Gb/s data. The pre-FEC SNR of the detected 16QAM constellations is measured at the receiver side, directly after DSP. First, the sole data channels under test are switched on, and the SNR is given in Figure 11(a), for the 100 first time units, and for both channels under test. The SNR for CUT1 is about 0.2 dB below CUT2. Then the sensing channel is switched on: it operates in a 50GHz spacing in ITU grid 51. The SNR is measured for 100 additional time units in Figure 11(a). Overall, the measured SNR after 82 km transmission is left unchanged while switching on and off the sensing signal.

Yet, the experiment in Figure 11(a) is performed with a 25 GHz frequency spacing between the sensing spectrum and the data on CUT1 and CUT2. Now the CUTs are brought closer and closer to the sensing signal, up to a 2 GHz spacing in Figure 11(b). It was not possible to perform smaller spacing due to the granularity limit of the WSS used in the experiment. The SNR performance of the channel 2 (centered around $f = 195.15$ THz in Figure 11(c)) remains stable as we approach the sensing signal down to 2 GHz. The SNR results are displayed for CUT2, although the conclusions are similar for CUT1. This result further demonstrated the non-intrusive coexistence of the digital sensing system with high-speed transmission data.

VI. OPTICAL INFRASTRUCTURE SENSING BEYOND DAS

DAS is not the only fibre sensing solution in an optical network. Forward-propagation based sensing configurations, though less sensitive, can also be used to detect and even localize vibrations. One bottleneck in optical networks is the presence of amplifiers which restricts the usage of DAS to a per-span sensing. To circumvent this limitation, a hybrid forward and backward sensing approach with a first level of forward-propagation based sensing can be envisioned. Then, a second level of backscattered-based sensing complements the first level by providing an accurate location and characterization the vibration event within the span.

Submarine lines are a specific case with ultra-long-distance capabilities enabled by the repeaters periodically installed along the link. According to the repeater architecture, which is manufacturer dependent, a small portion of the signal from each span can be transmitted to the line termination thanks to a specific link for monitoring purpose. In such a submarine architecture, implementing forward sensing would provide a coarse localization of events, equal to the span length, so enabling ideal complementarity with a per-span DAS approach. In [38], [39], continuous wave optical signals were sent back and forth through a fiber pair for vibration detection and localization by phase extraction and propagation time computation. In [39], an ultra-narrow coherent laser source was also required which is not available by default in an optical transmission system. Later, new demonstrations

showed how to convert the optical network infrastructure into a real-time vibration sensor without the use of a DAS system but using the existing network hardware and intelligence at network nodes, for instance at optical transceivers. In [40]–[43], different groups extracted the evolution of the state of polarization (SOP) or the phase of the propagating wave from the outputs of the digital equalizer of the coherent receiver. SOP or phase changes were monitored in the lab in [40], [41], and seismic and water waves were characterized over a 10,000km-long submarine cable connecting Los Angeles, USA, and Valparaiso in Chile in [42]. Localization of vibration events was based on the extraction of information from bidirectional WDM transmissions over deployed fiber cables [42]–[44].

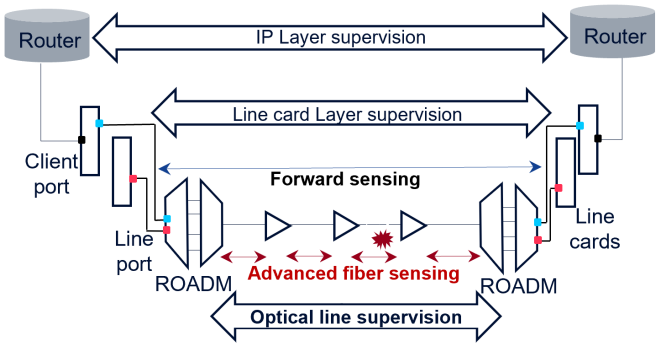

Fig. 12. Global network telemetry system including fiber sensing at the optical layer.

We believe that forward phase and SOP sensing and DAS approaches potentially complement each other and that they both form a fulsome vibration sensing solution for metropolitan and submarine coherent optical networks: DAS provides high sensitivity and accurate localisation of mechanical events over distances limited to span length, and multiple systems are thus needed to cover a full optical link ; conversely, forward sensing can monitor ultra-long distance links with a single system to detect high energy perturbations.

With regards to the constantly increasing amount of transported information and the growing impact of a network failure, telecom operators strive for monitoring their network with more and more accuracy [10]. Figure 12 displays the concept of a global telemetry system where in-depth monitoring is implemented at each network layer. In this figure, we show a scheme using DAS interrogators located at each amplification stage between two fiber spans, complemented by forward sensing over a full light path based on a collection of information available form the DSP of coherent transponders. For example, the DAS interrogators can be enabled on-demand in relation with forward sensing or upper layers alarms, so enabling accurate event localization and identification when required while generating a reasonable amount of sensing data.

VII. Conclusion

We intended to show that leveraging technologies used in coherent optical transmission as dual polarisation transceivers along with telecom dedicated digital signal processing allows to revisit Distributed Acoustic Sensing, further enhancing the detection threshold.

The polarisation diversity probing technique, yielding formally perfect estimation of the Rayleigh backscattered channel, is the backbone of this approach. Beyond solving the polarisation fading issue, it can be advantageously complemented by OFDM to mitigate in turn the coherent fading. Also, channel estimation under a Jones matrix form helps detect the remaining intensity drops, giving rise to soft decision reliability metric which locates potential phase artifacts and can be exploited further, to enhance classification of detected mechanical events.

The scalability with respect to the practical coherence limitation of the laser source was also discussed. Finally, it was shown experimentally that, thanks to the specific time spreading properties of the probing signal, such DAS system can coexist with data traffic in already deployed telecom networks without impacting transmission performance. Therefore, this innovative approach to DAS is an appealing potential basis for a future global telemetry system dedicated to optical networks.

References

[1] K. Hicke, M.-T. Hussels, R. Eisermann, S. Chruscicki, and K. Krebber, "Condition monitoring of industrial infrastructures using distributed fibre optic acoustic sensors," in *2017 25th Optical Fiber Sensors Conference (OFS)*. IEEE, 2017, pp. 1–4.

[2] W. Hill, J. J. Williams, and G. Lees, "Smart fiber-optic sensing systems enhance physical border walls and fences," *LASER FOCUS WORLD*, vol. 55, no. 7, pp. 23–26, 2019.

[3] M.-F. Huang, M. Salemi, Y. Chen, J. Zhao, T. J. Xia, G. A. Wellbrock, Y.-K. Huang, G. Milione, E. Ip, P. Ji, T. Wang, and Y. Aono, "First field trial of distributed fiber optical sensing and high-speed communication over an operational telecom network," *Journal of Lightwave Technology*, vol. 38, no. 1, pp. 75–81, 2020.

[4] G. Cedilnik, R. Hunt, and G. Lees, "Advances in train and rail monitoring with das," in *26th International Conference on Optical Fiber Sensors*. Optica Publishing Group, 2018, p. ThE35. [Online]. Available: http://opg.optica.org/abstract.cfm?URI=OFS-2018-ThE35

[5] S. Kowarik, M.-T. Hussels, S. Chruscicki, S. Münzenberger, A. Lämmerhirt, P. Pohl, and M. Schubert, "Fiber optic train monitoring with distributed acoustic sensing: Conventional and neural network data analysis," *Sensors*, vol. 20, no. 2, 2020. [Online]. Available: https://www.mdpi.com/1424-8220/20/2/450

[6] Victoria and S. D. Albert Museum. (2020) Big glass microphone project. [Online]. Available: https://www.vam.ac.uk/bigglassmic/#

[7] J. B. Ajo-Franklin, S. Dou, N. J. Lindsey, I. Monga, C. Tracy, M. Robertson, V. Rodriguez Tribaldos, C. Ulrich, B. Freifeld, T. Daley *et al.*, "Distributed acoustic sensing using dark fiber for near-surface characterization and broadband seismic event detection," *Scientific reports*, vol. 9, no. 1, pp. 1–14, 2019.

[8] N. J. Lindsey, S. Yuan, A. Lellouch, L. Gualtieri, T. Lecocq, and B. Biondi, "City-scale dark fiber das measurements of infrastructure use during the covid-19 pandemic," *Geophysical research letters*, vol. 47, no. 16, 2020.

[9] T. Zhu, J. Shen, and E. R. Martin, "Sensing earth and environment dynamics by telecommunication fiber-optic sensors: an urban experiment in pennsylvania, usa," *Solid Earth*, vol. 12, no. 1, pp. 219–235, 2021. [Online]. Available: https://se.copernicus.org/articles/12/219/2021/

[10] V. Vusirikala, "Optical networking long term vision: a hyperscaler perspective," *invited paper M1A. 3, OFC*, 2021.

[11] H. F. Martins, S. Martin-Lopez, P. Corredera, P. Salgado, O. Frazão, and M. González-Herráez, "Modulation instability-induced visibility fading in phase-sensitive OTDR," in *Fifth European Workshop on Optical Fibre Sensors*, L. R. Jaroszewicz, Ed., vol. 8794, International Society for Optics and Photonics. SPIE, 2013, pp. 538 – 541. [Online]. Available: https://doi.org/10.1117/12.2026062

[12] R. Goldman, A. Agmon, and M. Nazarathy, "Direct detection and coherent optical time-domain reflectometry with golay complementary codes," *Journal of Lightwave Technology*, vol. 31, no. 13, pp. 2207–2222, 2013.

[13] H. F. Martins, K. Shi, B. C. Thomsen, S. Martin-Lopez, M. Gonzalez-Herraez, and S. J. Savory, "Real time dynamic strain monitoring of optical links using the backreflection of live PSK data," *Optics Express*, vol. 24, no. 19, p. 22303, 2016. [Online]. Available: https://www.osapublishing.org/abstract.cfm?URI=oe-24-19-22303

[14] C. Dorize and E. Awwad, "Enhancing the performance of coherent OTDR systems with polarization diversity complementary codes," *Optics Express*, vol. 26, no. 10, p. 12878, 2018. [Online]. Available: https://www.osapublishing.org/abstract.cfm?URI=oe-26-10-12878

[15] SEAFOM, *DAS Parameter Definitions and Tests*, measuring sensor performance-02 ed., http://seafom.com, 2018.

[16] S. Guerrier, C. Dorize, E. Awwad, and J. Renaudier, "Introducing coherent MIMO sensing, a fading-resilient, polarization-independent approach to ϕ-OTDR," *Optics Express*, vol. 28, no. 14, p. 21081, 2020. [Online]. Available: https://www.osapublishing.org/abstract.cfm?URI=oe-28-14-21081

[17] R. C. Jones, "A new calculus for the treatment of optical SystemsV a more general formulation, and description of another calculus," *Journal of the Optical Society of America*, vol. 37, no. 2, p. 107, 1947. [Online]. Available: https://www.osapublishing.org/abstract.cfm?URI=josa-37-2-107

[18] C. Dorize, S. Guerrier, E. Awwad, P. A. Nwakamma, H. Mardoyan, and J. Renaudier, "An OFDM-MIMO distributed acoustic sensing over deployed telecom fibers," in *Optical Fiber Communication Conference*, 2021, p. 3.

[19] E. Awwad, C. Dorize, S. Guerrier, and J. Renaudier, "Detection-localization-identification of vibrations over long distance SSMF with coherent delta-phi-OTDR," *Journal of Lightwave Technology*, vol. 38, no. 12, pp. 3089 – 3095, 2020, conference Name: Journal of Lightwave Technology.

[20] Q. Yan, M. Tian, X. Li, Q. Yang, and Y. Xu, "Coherent ϕ-OTDR based on polarization-diversity integrated coherent receiver and heterodyne detection," in *2017 25th Optical Fiber Sensors Conference (OFS)*, 2017, pp. 1–4.

[21] P. Healey, "Fading in heterodyne otdr," *Electronics Letters*, vol. 20, no. 1, pp. 30 – 32, 1984.

[22] C. Dorize, S. Guerrier, E. Awwad, and J. Renaudier, "Identification of rayleigh fading induced phase artifacts in coherent differential ϕ-OTDR," *Optics Letters*, vol. 46, no. 11, p. 2754, 2021. [Online]. Available: https://www.osapublishing.org/abstract.cfm?URI=ol-46-11-2754

[23] A. H. Hartog, L. B. Liokumovich, N. A. Ushakov, O. I. Kotov, T. Dean, T. Cuny, A. Constantinou, and F. V. Englich, "The use of multi-frequency acquisition to significantly improve the quality of fibre-optic-distributed vibration sensing," *Geophysical Prospecting*, vol. 66, pp. 192–202, 2018, _eprint: https://onlinelibrary.wiley.com/doi/pdf/10.1111/1365-2478.12612. [Online]. Available: https://onlinelibrary.wiley.com/doi/abs/10.1111/1365-2478.12612

[24] M. J. Murray and B. Redding, "Quantitative amplitude-measuring ϕ-OTDR with $\mathrm{p}\epsilon/\sqrt{Hz}$ sensitivity using a multi-frequency pulse train," *Optics Letters*, vol. 45, no. 18, p. 5226, 2020. [Online]. Available: https://www.osapublishing.org/abstract.cfm?URI=ol-45-18-5226

[25] F. Pang, M. He, H. Liu, X. Mei, J. Tao, T. Zhang, X. Zhang, N. Chen, and T. Wang, "A fading-discrimination method for distributed vibration sensor using coherent detection of $\varphi $ -OTDR," *IEEE Photonics Technology Letters*, vol. 28, no. 23, pp. 2752–2755, 2016, conference Name: IEEE Photonics Technology Letters.

[26] S. Lin, Z. Wang, J. Xiong, Y. Fu, J. Jiang, Y. Wu, Y. Chen, C. Lu, and Y. Rao, "Rayleigh fading suppression in one-dimensional optical scatters," *IEEE Access*, vol. 7, pp. 17 125–17 132, 2019.

[27] S. Guerrier, C. Dorize, E. Awwad, and J. Renaudier, "A fully digital MIMO-OFDM scheme for fading mitigation in coherent $\delta\phi$-OTDR," *Optics Express*, 2021, publisher: Optical Society of America. [Online]. Available: https://www.osapublishing.org/oe/abstract.cfm?msid=

[28] M. Zabihi, Y. Chen, T. Zhou, J. Liu, Y. Shan, Z. Meng, F. Wang, Y. Zhang, X. Zhang, and M. Chen, "Continuous fading suppression method for ϕ-OTDR systems using optimum tracking over multiple probe frequencies," *Journal of Lightwave Technology*, vol. 37, no. 14, pp. 3602–3610, 2019. [Online]. Available: https://ieeexplore.ieee.org/document/8720050/

[29] D. Chen, Q. Liu, and Z. He, "Phase-detection distributed fiber-optic vibration sensor without fading-noise based on time-gated digital OFDR," *Optics Express*, vol. 25, no. 7, p. 8315, 2017. [Online]. Available: https://www.osapublishing.org/abstract.cfm?URI=oe-25-7-8315

[30] J. Pastor-Graells, H. F. Martins, A. Garcia-Ruiz, S. Martin-Lopez, and M. Gonzalez-Herraez, "Single-shot distributed temperature and strain tracking using direct detection phase-sensitive OTDR with chirped pulses," *Optics Express*, vol. 24, no. 12, pp. 13 121–13 133, 2016, publisher: Optical Society of America. [Online]. Available: https://www.osapublishing.org/oe/abstract.cfm?uri=oe-24-12-13121

[31] A. E. Alekseev, V. S. Vdovenko, B. G. Gorshkov, V. T. Potapov, and D. E. Simikin, "A phase-sensitive optical time-domain reflectometer with dual-pulse diverse frequency probe signal," *Laser Physics*, vol. 25, no. 6, p. 065101, 2015. [Online]. Available: http://stacks.iop.org/1555-6611/25/i=6/a=065101?key=crossref.19340bfa134f8512a070754d53619108

[32] Z. Jia, L. A. Campos, M. Xu, H. Zhang, M. Gonzalez-Herraez, H. F. Martins, and Z. Zhan, "Experimental coexistence investigation of distributed acoustic sensing and coherent communication systems," in *Optical Fiber Communication Conference (OFC) 2021*. Optica Publishing Group, 2021, p. Th4F.4. [Online]. Available: http://opg.optica.org/abstract.cfm?URI=OFC-2021-Th4F.4

[33] U. Rohrs and L. Linde, "Some unique properties and applications of perfect squares minimum phase cazac sequences," in *Proceedings of the 1992 South African Symposium on Communications and Signal Processing*. IEEE, 1992, pp. 155–160.

[34] C. Dorize, E. Awwad, S. Guerrier, and J. Renaudier, "Optimal probing sequences for polarization-multiplexed coherent phase OTDR," in *Optical Fiber Sensors Conference 2020 Special Edition*. OSA, 2021, p. T3.23. [Online]. Available: https://www.osapublishing.org/abstract.cfm?URI=OFS-2020-T3.23

[35] A. E. Alekseev, Y. A. Tezadov, and V. T. Potapov, "Statistical properties of backscattered semiconductor laser radiation with different degrees of coherence," *Quantum Electronics*, vol. 42, no. 1, pp. 76–81, 2012. [Online]. Available: http://stacks.iop.org/1063-7818/42/i=1/a=A15?key=crossref.792760607f67a607fd284cf05aff5cf3

[36] M.-F. Huang, M. Salemi, Y. Chen, J. Zhao, T. J. Xia, G. A. Wellbrock, Y.-K. Huang, G. Milione, E. Ip, P. Ji, T. Wang, and Y. Aono, "First field trial of distributed fiber optical sensing and high-speed communication over an operational telecom network," *Journal of Lightwave Technology*, vol. 38, no. 1, pp. 75–81, 2020.

[37] S. Guerrier, K. Benyahya, C. Dorize, E. Awwad, H. Mardoyan, and J. Renaudier, "Vibration detection and localization in buried fiber cable after 80km of SSMF using digital coherent sensing system with co-propagating 600gb/s WDM channels," in *Optical Fiber Communication Conference (OFC) 2022 (2022), paper M2F.3*. Optica Publishing Group, 2022, p. M2F.3. [Online]. Available: https://opg.optica.org/abstract.cfm?uri=OFC-2022-M2F.3

[38] I. D. Luch, P. Boffi, and R. Gaudino, "Vibration sensing for deployed metropolitan fiber infrastructure," *JOURNAL OF LIGHTWAVE TECHNOLOGY*, vol. 39, no. 4, p. 8, 2021.

[39] G. Marra, C. Clivati, R. Luckett, A. Tampellini, J. Kronjäger, L. Wright, A. Mura, F. Levi, S. Robinson, A. Xuereb, B. Baptie, and D. Calonico, "Ultrastable laser interferometry for earthquake detection with terrestrial and submarine cables," *Science*, p. eaat4458, 2018. [Online]. Available: http://www.sciencemag.org/lookup/doi/10.1126/science.aat4458

[40] F. Boitier, V. Lemaire, J. Pesic, L. Chavarria, P. Layec, S. Bigo, and E. Dutisseuil, "Proactive fiber damage detection in real-time coherent receiver," in *2017 European Conference on Optical Communication (ECOC)*, 2017, pp. 1–3.

[41] F. Boitier, J. Pesic, V. Lemaire, E. Dutisseuil, J. M. E. Tolosa, P. Jennevé, N. L. Moing, H. Mardoyan, and P. Layec, "Seamless optical path restoration with just-in-time resource allocation leveraging machine learning," in *2018 European Conference on Optical Communication (ECOC)*, 2018, pp. 1–3.

[42] Z. Zhan, M. Cantono, V. Kamalov, A. Mecozzi, R. Müller, S. Yin, and J. C. Castellanos, "Optical polarization–based seismic and water wave sensing on transoceanic cables," *Science*, vol. 371, no. 6532, pp. 931–936, 2021. [Online]. Available: https://www.science.org/doi/10.1126/science.abe6648

[43] E. Ip, Y.-K. Huang, G. Wellbrock, T. Xia, M.-F. Huang, T. Wang, and Y. Aono, "Vibration detection and localization using modified digital coherent telecom transponders," *Journal of Lightwave Technology*, vol. 40, no. 5, pp. 1472–1482, 2022. [Online]. Available: https://ieeexplore.ieee.org/document/9665265/

[44] M. Mazur, J. C. Castellanos, R. Ryf, E. Börjeson, T. Chodkiewicz, V. Kamalov, S. Yin, N. K. Fontaine, H. Chen, L. Dallachiesa, S. Corteselli, P. Copping, J. Gripp, A. Mortelette, B. Kowalski, R. Dellinger, D. T. Neilson, and P. Larsson-Edefors, "Transoceanic phase and polarization fiber sensing using real-time coherent transceiver," in *2022 Optical Fiber Communications Conference and Exhibition (OFC)*, 2022, pp. 1–3.